Int. J. Electrochem. Sci., 12 **(2017)** 2822 – 2835, doi: 10.20964/2017.04.32

International Journal of
ELECTROCHEMICAL
SCIENCE
www.electrochemsci.org

High-rate-capability Graphene Oxide/$Li_4Ti_5O_{12}$-composite Anode for Lithium-Ion Batteries

Wen Li[1,2,*], *Aijia Wei*[1,2], *Xiaohui Li*[1,2], *Lihui Zhang*[1,2], *Hao Wang*[3], *Wujie Ge*[3], *Zhenfa Liu*[1,2,*]

[1] Institute of Energy Resources, Hebei Academy of Science, Shijiazhuang, Hebei Province 050081, PR China.
[2] Hebei Engineer Research Center for Water Saving in Industry, Shijiazhuang, Hebei Province 050081, PR China
[3] Chengdu Institute of Organic Chemistry, Chinese Academy of Sciences, Chengdu 610041, PR China
[*]E-mail: liwen_cc@yeah.net, liuzhenfa@hebut.edu.cn

Received: 12 December 2016 / *Accepted:* 9 February 2017 / *Published:* 12 March 2017

A graphene oxide/$Li_4Ti_5O_{12}$ (GO/LTO) composite was prepared with 1 wt% GO and 99 wt% commercial LTO by stirring at a high speed and then drying at a low temperature. Compared with pure LTO, the GO/LTO composite demonstrated higher charge capacity and better rate capability over 0-3 V. The charge capacities at 0.5, 1, 3, 5, and 10 C were 246.3, 234.0, 223.2, 220.6, and 214.1 mAh g^{-1}, respectively, for GO/LTO and 233.7, 218.7, 202.1, 190.5, and 148.5 mAh g^{-1}, respectively, for LTO. Furthermore, the GO/LTO composite retained 95.1% of the initial capacity after 200 cycles at a high rate of 5 C, which was considerably higher than that that retained by the pure LTO (57.9%). The greatly improved electrochemical performance is attributed to an enhancement of lithium ion and electron conductivity caused by GO addition. GO acts as a binder, thereby improving the adhesive power of the electrode materials to the current collector. The electrode polarization is reduced and the electrolyte reduction decomposition is partially suppressed by adding GO. The process of preparing the GO/LTO composite is simple, low-cost and suitable for industrial use.

Keywords: graphene oxide, $Li_4Ti_5O_{12}$, composite, lithium-ion batteries

1. INTRODUCTION

The spinel $Li_4Ti_5O_{12}$ **(**LTO) is suggested as one of the most promising anode materials to replace graphite in large-scale lithium ion batteries (LIBs) for application in electric vehicle and hybrid electric vehicle power sources, due to its promising properties: zero volume change during charge/discharge, high working potential of the Ti^{4+}/Ti^{3+} redox couple (ca. 1.55 V vs. Li/Li^+), absence of SEI-layer formation and metallic lithium, excellent safety and thermal stability, and long cycle life

within a wide range of operating temperatures [1-4]. Unfortunately, LTO shows a low intrinsic electronic conductivity and lithium-ion diffusion coefficient, which seriously hinders its high-rate performance [5]. A number of approaches have been used to overcome these problems in attempts to improve the electrochemical performance of LTO anodes, including morphological optimization [6-20], nanostructuring [21-25], doping [26-37], surface coating [38-44] and formation of composite [45-54]. Among these methods above, preparation of LTO-based composites by adding high conductive carbon materials via a facile route is practicable and economical for large-scale industrialization.

To our best knowledge, graphene as a carbon resource usually fabricated by reducing graphene oxide (GO), has attracted intense attention recently [55]. Due to its superior electrical conductivity and high specific surface area (>2600 m^2 g^{-1}), graphene has been used to prepare the LTO/graphene composites to enhance the electrochemical properties of LTO [56-62]. The added graphene could avoid aggregation of the LTO particles, increase the apparent conductivity of the electrode and provide large active contact area between the electrode and electrolyte, thereby improving the electrode performance, especially its rate capability [56-64]. As the precursor of graphene, GO also presents a higher lithium storage capacity and the preparation of GO is simpler and lower cost than graphene itself because it does not need a reduction treatment [65-66]. However, GO and GO-based composites direct used as anode materials in LIBs are hardly reported. We have previously used GO to prepare graphite/GO composites and GO/graphite/carbon composites as anode materials. These anode materials demonstrated good electrochemical performance, including a higher storage capacity than traditional graphite anode materials [66-67]. Moreover, GO has been found lithium to easily form self-assembled membranes and can be used instead of a polymer binder in electrodes [66-67]. Thus, commercial LTO, GO, and conductive carbon black were recently applied to fabricate a binder-free GO/LTO composite as an anode material in our work [68]. The addition of GO provides the additional capacity via oxygen-containing functional group and nano-cavity [68-69]. In addition to contributing to the lithium-ion storage, GO also acted as a binder, replacing the carboxy methylated cellulose, which makes the composite with CMC binder free, thereby speeding up the lithium ion diffusion in anode materials [68].

Unfortunately, the binder-free GO/LTO composite required more than 10 wt% GO to obtain outstanding electrode adhesion and electrochemical performance, which is prohibitive due to the high cost of GO. In this study, we used a simple method that required only 1 wt% GO mixed with 99 wt% commercial LTO to prepare a novel GO/LTO composite material and investigated this material for use as a lithium battery anode.

2. EXPERIMENTAL

2.1. Synthesis and characterization

GO was synthesized from high-purity natural flake graphite (about 200 mesh, Changsha Shenghua Research Institute, 99.999%) by a modified Hummers method [66-68]. A colloidal dispersion of GO in deionized water was prepared by ultrasonication (20 kHz ultrasound probe)

treatment for about 30 min to give a stable amber dispersion [68]. Commercial LTO powder (Shanghai Dian Yang Industrial Co., Ltd.) was then added to the aqueous GO dispersion and stirred for 4 h at a linear velocity of 18 m per s Finally, the mixture was dried at 105 °C to obtain the GO/LTO composite.

Powder X-ray diffraction (XRD, Xpert MPD DY1219) with Cu K_α radiation was used to identify the phase composition of the materials. The diffraction patterns were collected at room temperature by step scanning over a 10-90° range at a scanning rate of 0.02° per 10 s. The morphology of the materials was determined using scanning electron microscopy (SEM, Sirion 200 FEI Netherlands) and high-resolution transmission electron microscopy (TEM, JEM-100CX, JEOL).

2.2. Electrochemical measurements

The electrochemical properties of the prepared materials were measured using a CR2032 coin-type half-cell in which the cathode and Li-metal anode were separated by a porous polypropylene film (Celgard 2400, Celgard Inc., USA). The cathode slurry was prepared by homogeneously mixing the active material (LTO or GO/LTO), Super-P carbon black, and LA-132 binder in a mass ratio of 85:5:5 in deionized water. Then the slurry was cast onto a Cu foil and dried for 12 h under vacuum at 105 °C. Finally, the electrode laminate was punched into disks (10 mm in diameter) and dried in a vacuum oven at 105 °C for 24 h. The coin-cell assembly was performed in an argon-filled glovebox. A solution of 1 mol L^{-1} $LiPF_6$ in ethylene carbonate, dimethyl carbonate, and diethyl carbonate (1:1:1, in volume) was used as the electrolyte (Shenzhen Capchem Technology (Shenzhen) Co., Ltd.).

Galvanostatic charge-discharge tests were conducted over 0-3 V at different charge/discharge C-rates between 0.2 and 10 C (1 C = 250 mAh g^{-1}) at 25 °C using an automatic galvanostatic charge-discharge unit (Land 2001A, Wuhan, China). An electrochemical workstation (PARSTAT 2273, USA) was used to carry out cyclic voltammetry (CV) and electrochemical impedance spectroscopy (EIS) tests. The CV tests were carried out over 0-3 V at a scan rate of 0.2 mV s^{-1}. The EIS measurements were performed over a frequency range of 10 mHz to 100 kHz at the stable voltage of 1.55 V during the first charge cycle.

3. RESULTS AND DISCUSSION

Fig. 1 shows the standard XRD pattern of LTO and XRD patterns of the LTO used here and the GO/LTO composite. The diffraction peaks of the pure LTO and GO/LTO samples are both in agreement with the standard XRD pattern of LTO (ICSD No. 49-0207), suggesting the addition of GO and the calcination process had no effect on the crystal structure of LTO. Fig. 2 displays SEM micrographs of both samples. It can be seen from Fig. 3 that the particle size distribution of commercial LTO is about 0.5-1 μm, and there are some GO sheets among the LTO particles in the LTO/GO composite (Fig. 2b). The amount of GO in GO/LTO was about 1 wt% and, thus, only a few GO sheets can be seen among the LTO particles. Fig. 3 exhibits TEM micrographs of GO and the GO/LTO composite.

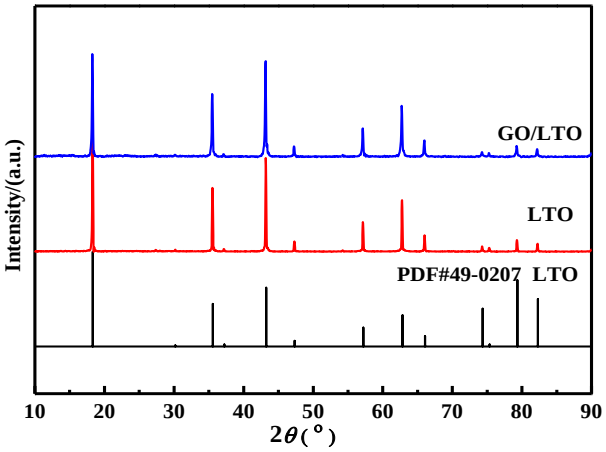

Figure 1. The standard XRD pattern of LTO and XRD patterns of both samples

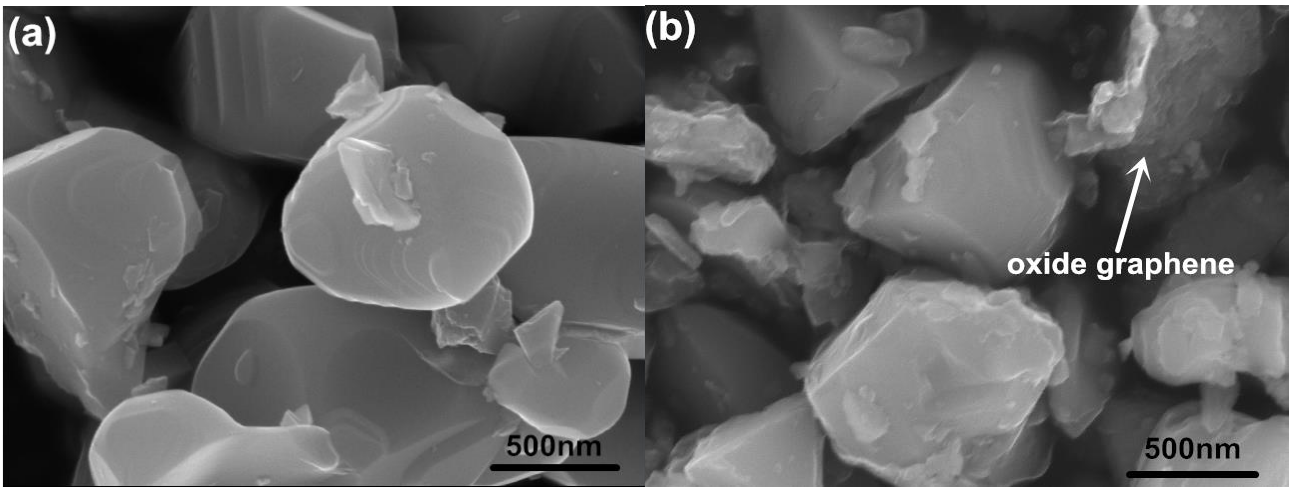

Figure 2. SEM micrographs of (a) LTO and (b) GO/LTO

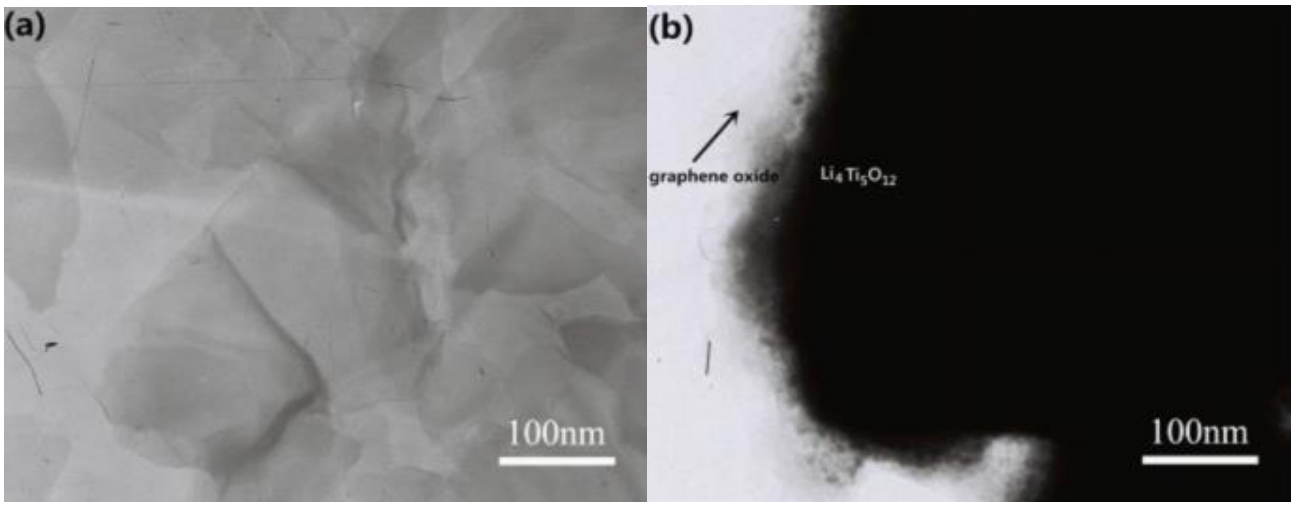

Figure 3. TEM micrographs of (a) GO and (b) GO/LTO

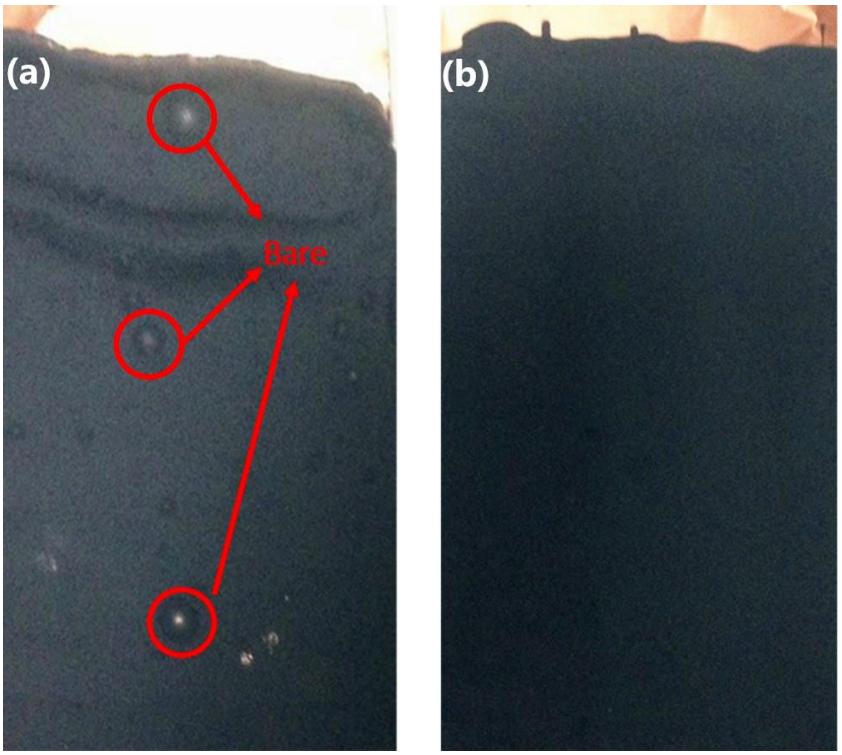

Figure 4. Photographs of (a) LTO and (b) GO/LTO electrodes

The GO appears as thin sheets (Fig. 3a), while GO sheets cover the LTO particles in the GO/LTO composite (Fig. 3b). Photographs of LTO and GO/LTO electrodes prepared under the same conditions are shown in Fig. 4.

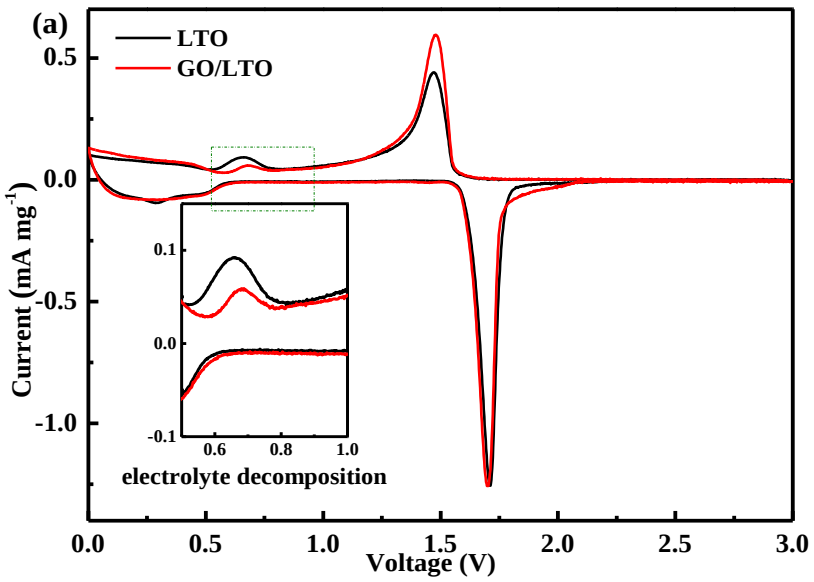

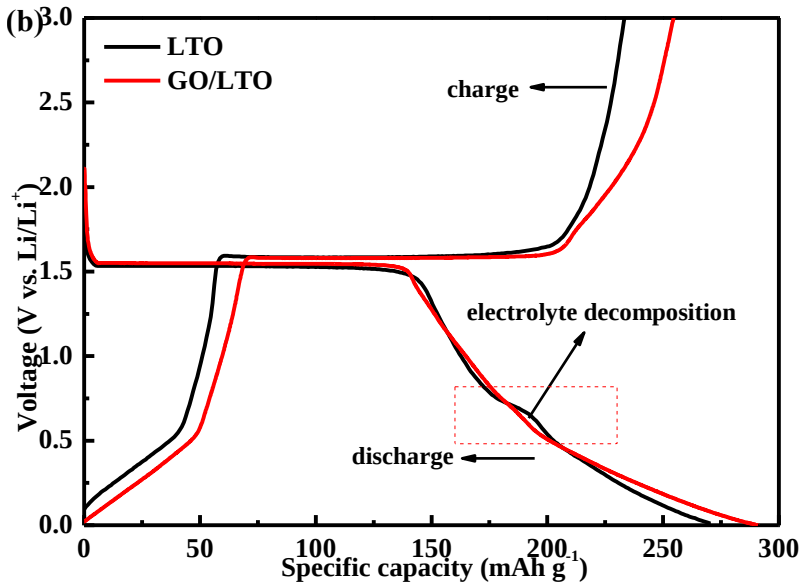

Figure 5. (a) CV curves of both samples at a scanning of 0.2 mV s^{-1} and (b) discharge-charge curves of both samples at 0.2 C-rate (1 C = 250 mAh g-1) over 0-3 V

The pure LTO electrode is unevenly coated with some bare Cu foil visible, but the GO/LTO electrode is perfectly coated with no bare Cu foil visible. This is a result of the added GO acts as a binder and enhancing the bond strength between the Cu foil and the electrode materials.

The electrochemical properties of both LTO and GO/LTO electrodes in the range of 0-3 V were systematically studied. Fig. 5a shows the CV curves of both electrodes over a 0-3 V range at a scan of 0.2 mV s^{-1}. The cathodic and anodic peaks at around 1.6 and 1.5 V, respectively, are attributed to the Ti^{4+}/Ti^{3+} redox couple, and the reduction and oxidation peaks below 0.6 V are caused by the further reduction of Ti^{4+} [69-70]. Moreover, for both samples, an obvious irreversible peak appears at around 0.7 V during the reduction process.

This is due to a reduction decomposition of the electrolyte on the LTO particles [69-70]. He et al prepared LTO and amorphous carbon-coated LTO materials with good electrochemical performance and investigated the reduction reactivity of electrolyte on both electrodes [70]. They found that a relatively thick SEI film was formed on both LTO electrodes after discharge-charge cycling up to 0 V, whereas only a very thin SEI film could be formed after discharge-charge cycling up to 1 V. However, the thinner SEI film formed on the LTO particles presented richer pores than that on the carbon-coated LTO particles, which provided open ways for a new reduction of electrolyte in contact with LTO surfaces. Thus, the electrolyte reduction on the carbon-coated LTO electrode could be suppressed effectively due to the continuous and dense SEI film formed on the surface of LTO particles. In contrast, the irreversible peak at around 0.7 V is slightly weaker for GO/LTO than LTO, suggesting the electrolyte reduction decomposition on the LTO particles is partly suppressed by the presence of GO. This is likely a result of the GO sheets covering a portion of the active sites on the surface of the LTO particles and preventing the electrolyte reduction decomposition. However, the GO sheets will also exist between the LTO particles rather than simply coating the surface, leading to incomplete suppression of the electrolyte reduction decomposition.

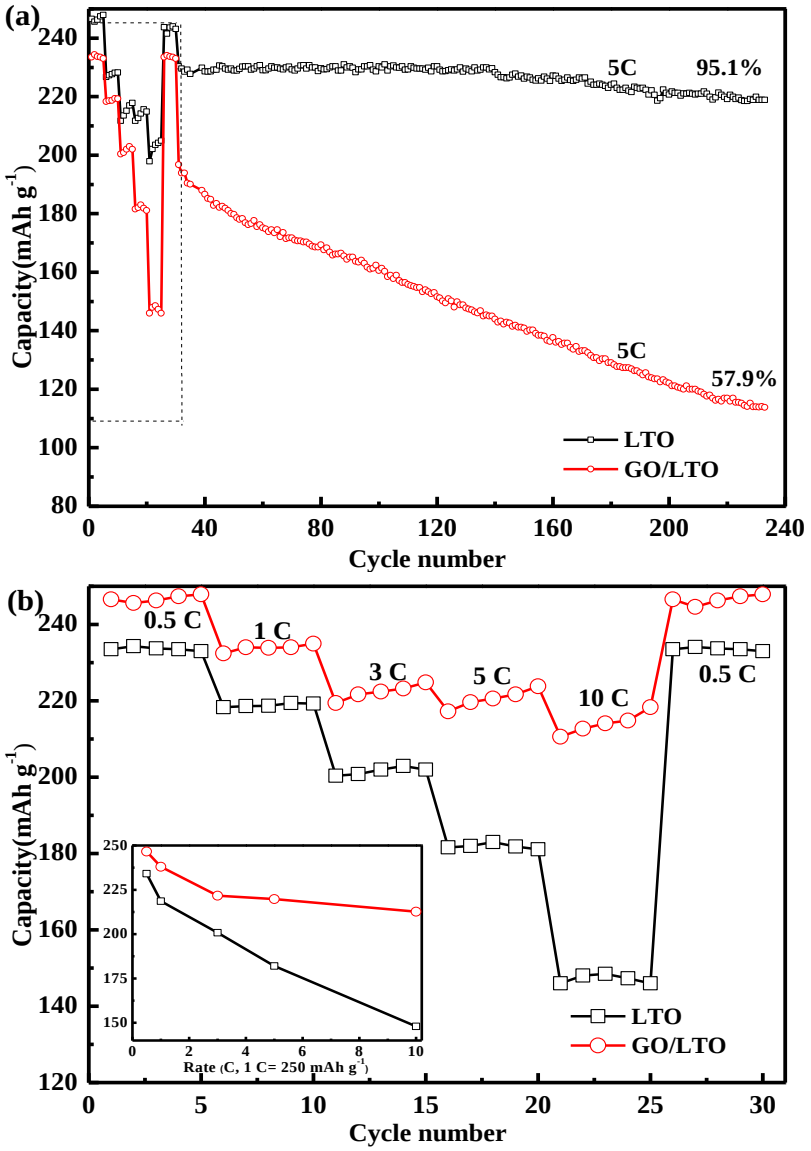

Figure 6. (a) Cycling performance and (b) rate capacity at various C-rates over 0-3 V and discharge capacity as a function of the C-rates (inset Fig. 6b) over 0-3 V of both samples (1 C = 250 mAh g^{-1})

Galvanostatic discharge-charge curves of both electrodes over 0-3 V at 0.2 C-rate for the first cycle are shown in Fig. 5b. Both samples demonstrate a large range of flat voltage at around 1.5 V during the discharge process and around 1.6 V during the charge process, which are assigned to Li^+ insertion and de-insertion, respectively, during a two-phase reaction and correspond to the pair of strong redox peaks around 1.6 and 1.5 V in the CV curves shown in Fig. 5a. Moreover, LTO shows a small range of flat voltage at around 0.7 V during the discharge process, which is attributed to the electrolyte reduction decomposition [69-70]. The flat-voltage range at around 0.7 V disappears for the GO/LTO composite electrode, showing that the electrolyte reduction decomposition is likely to be suppressed upon GO addition, which is in agreement with the CV data. The discharge curve of LTO can be separated into two sections, 3.0-1.0 V region and 1.0-0 V region, with the total specific

discharge capacity of 270.6 mAh g^{-1}, which is close to the results of reported work [71]. In the region above 1.0 V, the discharge capacity of 162.1mAh g^{-1} is corresponding to the transition from the spinel (LTO) to the rock-salt structure ($Li_7Ti_5O_{12}$). And in the section below 1.0 V, the discharge capacity is 108.5 mAh g^{-1}, which is higher than the theoretic capacity for the single phase transition from $Li_7Ti_5O_{12}$ to $Li_{8.5}Ti_5O_{12}$ (about 87.5 mAh g^{-1}) [71]. The extra capacity is mainly attributed to the lithium storage in the conductive carbon black and to the side reaction between the electrolyte and the electrode [71]. For the GO/LTO composite, the discharge curve is similar as that for pure LTO. In the first section (3.0-1.0 V), the discharge capacity is 164.7 mAh g^{-1}, which is nearly equal to that of the pure LTO. However, in the following section (1.0-0 V), the discharge capacity of 126.3 mAh g^{-1} is relatively higher than that of pure LTO (108.5 mAh g^{-1}). Comparing with LTO, the extra discharge capacity of the GO/LTO composite can be due to the lithium storage in the added GO. Xiang etal reported the LTO/graphene composite contains about 8 wt% garphene sheets showed a total discharge capacity of over 430 mAh g^{-1}, but a really low coulombic efficiency of 65.8% [71], which could be ascribed to the more side reactions on the active graphene sheets with high specific surface area [66-68, 71]. Whereas, the GO/LTO composite shows a relative higher coulombic efficiency of 87.5%, which is due to the less addition amount of GO.

Fig. 6a shows the cycling performance of both electrodes over 0-3 V and one can see that the GO/LTO composite exhibits significantly better cycling stability than pure LTO. The capacity retention of the GO/LTO composite electrode at a high rate of 5 C from cycles 35-230 is 95.1%, which is much higher than that of the pure LTO electrode (57.9%). Fig. 6b shows the rate capacity of both samples at various C-rates over 0-3 V, and the second-cycle discharge capacity at each rate is compared in the inset of Fig. 6b. The charge capacity decreased with increasing C-rate for both samples. The respective charge capacities at 0.5, 1, 3, 5, and 10 C are 233.7, 218.7, 202.1, 190.5 and 148.5 mAh g^{-1} for pure LTO and 246.3, 234.0, 223.2, 220.6 and 214.1 mAh g^{-1} for the GO/LTO composite, demonstrating that the charge capacity of GO/LTO was better than that of LTO at all tested C-rates.

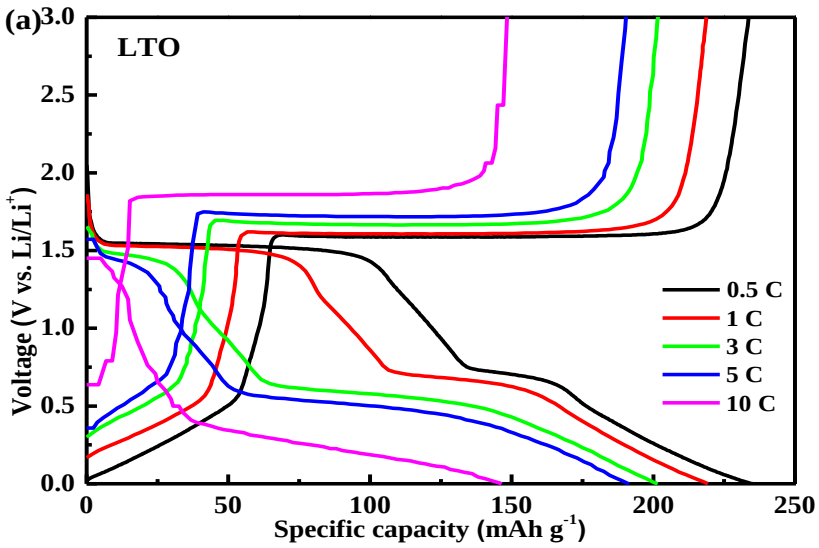

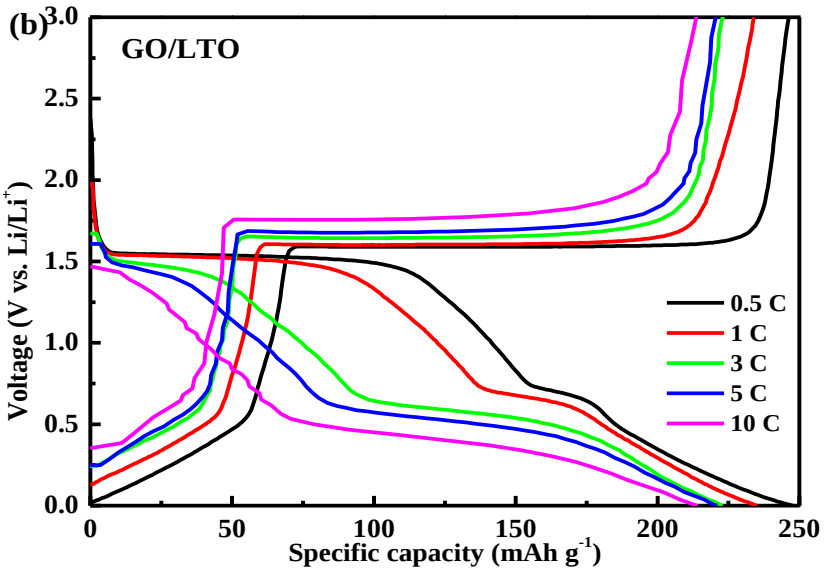

Figure 7. Discharge-charge curves of (a) LTO and (b) GO/LTO at different C-rates over 0-3 V

In our previous report, the pure LTO is co-modified with Mg^{2+} and F^- and the electrochemical performance in the range of 0-3 V was studied [69]. The charge capacities of Mg^{2+} and F^- co-modified LTO at 0.5C, 1C, 3C, 5C and 10C rate were 234.1, 218.6, 200.8, 182 and 148mAh g^{-1}, respectively [69]. Therefore, the GO/LTO composite electrode exhibits better rate capability than the Mg^{2+} and F^- co-modified LTO.

Table 1. Potential differences (△V, V) between discharge voltage platform($\varphi_{discharge}$, V) and charge voltage platform (φ_{charge}, V) at different C-rates

C-rate	LTO			GO/LTO		
	$\varphi_{discharge}$	φ_{charge}	$\triangle V$	$\varphi_{discharge}$	φ_{charge}	$\triangle V$
0.5 C	1.548	1.594	0.046	1.550	1.591	0.041
1 C	1.532	1.611	0.079	1.541	1.604	0.063
3 C	1.477	1.673	0.196	1.506	1.645	0.139
5 C	1.439	1.723	0.284	1.476	1.678	0.202
10 C	1.271	1.860	0.589	1.389	1.756	0.367

Fig. 7 shows the discharge-charge curves of both samples at different C-rates over 0-3 V. For both electrodes, it can be seen that the potential difference between discharge and charge voltage platforms becomes larger with increasing C-rate, suggesting increased electrode polarization at higher C-rates. Table 1 lists the values of discharge voltage platforms ($\varphi_{discharge}$), charge voltage platforms (φ_{charge}) and potential difference between discharge and charge voltage platforms ($\triangle V$) at different C-rates. The GO/LTO presents lower φ_{charge} than LTO, especially at high C-rates, which is benefit for improving energy density of lithium ions batteries using LTO as anode material. The values of $\triangle V$ are

smaller for the GO/LTO composite electrode compared to the pure LTO electrode at all tested C-rates, which indicates that adding GO reduces the electrode polarization.

EIS is considered to be one of the most sensitive tools for studying changes in electrode behavior. The results of EIS measurements at the stable voltage of 1.55 V are shown in Fig. 8 for all samples. The impedance spectra in Fig. 8a are composed of one semicircle at higher frequencies followed by a linear section at lower frequencies [69-70]. The low frequency region of the straight line is attributed to the diffusion of lithium ions into the bulk of the electrode material, the so-called Warburg diffusion [69-70]. The relationship between the imaginary impedance and the low frequencies is illustrated in Fig. 8b. This relationship is governed by Eqs. (1) and (2). Diffusion coefficient values for the lithium ions in the bulk electrode materials are calculated by Eq. (3). The exchange current density *i* is obtained by Eq. (4).

$$Z'' = -\sigma\omega^{-0.5}, \quad [1]$$

$$Z_{re} = R_s + R_{ct} + \sigma_\omega \omega^{-0.5}, \quad [2]$$

$$D = 0.5\left(\frac{RT}{AF^2\sigma_\omega C}\right)^2, \quad [3]$$

$$i = \frac{RT}{nFR_{ct}}, \quad [4]$$

where Z'' is the imaginary impedance, ω is the angular frequency in the low frequency region, R_s is the electrolyte resistance, R_{ct} is the charge-transfer resistance, R is the gas the gas constant; D is the diffusion coefficient; T is the absolute temperature; F is Faraday's constant; A is the area of the electrode surface; C is the molar concentration of lithium ions and i is the exchange current density. The EIS parameters are stated in Table 2.

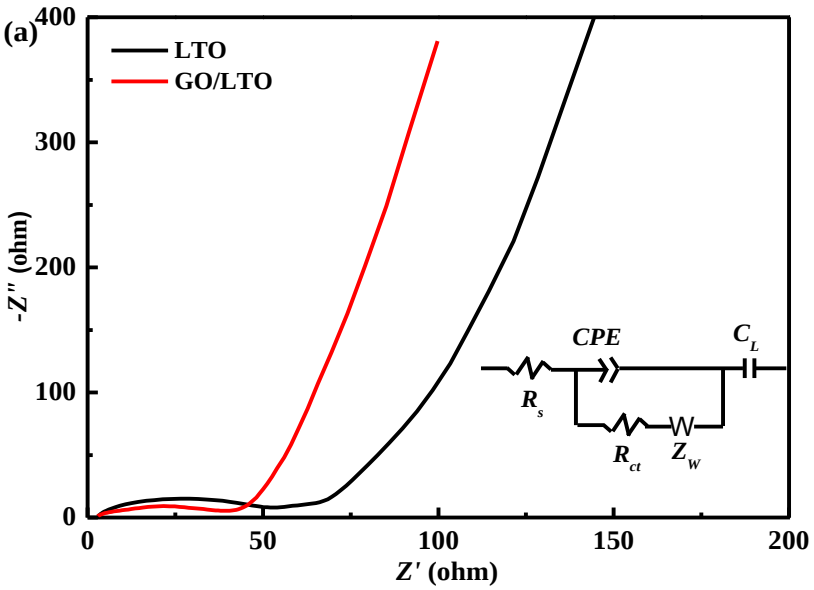

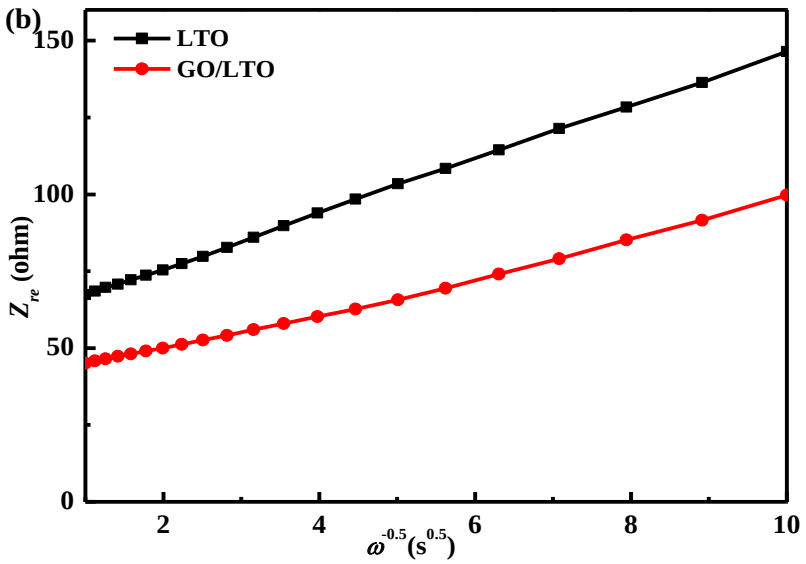

Figure 8. (a) EIS curves and (b) the relationship between Z_{re} and the lower angular frequencies of both samples

Table 2. The EIS parameters of both samples

Sample	R_s (Ω)	R_{ct} (Ω)	$\omega^{-0.5}$ (Ω cm^2 s^{-1})	D (cm^2 s^{-1})	i (mA cm^{-2})
LTO	2.89	51.13	8.78	1.83E-9	1.96E-3
GO/LTO	2.91	36.29	6.08	3.82E-9	2.76E-3

The value of D for the GO/LTO composite is higher than that of pure LTO, indicating that lithium ions have greater mobility within the GO/LTO composite than within pure LTO. Furthermore, the value of i for the GO/LTO composite is also higher than that of pure LTO, suggesting that the charge-transfer reaction is stronger for the GO/LTO composite electrode than the pure LTO electrode. Therefore, the GO/LTO composite has better ionic and electronic conductivity than pure LTO. This is likely to be due to the following factors: (1) The added GO acts as a binder and enhances the adhesion of the electrode materials to the current collector, thereby improving the transport of lithium ions and electrons among the electrode materials; (2) The GO sheets cover a portion of the catalytic sites for decomposition of electrolyte, thereby suppressing SEI layer formation and effectively accelerating the diffusing of lithium ions and electrons to the electrode surface when compared with the SEI-layer-coated LTO electrode.

4. CONCLUSION

GO acts as binder in the GO/LTO composite, thereby improving the adhesion of the electrode materials to the current collector. The electrochemical results demonstrate that the electrode polarization is reduced and the electrolyte reduction-decomposition is partially suppressed by adding

GO. Meanwhile, the GO/LTO composite exhibits higher lithium ion and electron conductivity than pure LTO. Hence, the GO/LTO composite shows superior rate capability and cycling performance over 0-3 V compared with pure LTO. In particular, the GO/LTO composite retains 95.1% of the initial capacity after 200 cycles at a high rate of 5 C.

ACKNOWLEDGEMENTS
This work was financially supported by Science and Technology Program of Hebei Province (16294403D) and Project of Hebei Academy of Science (161302).

References

1. B. Yan, M. Li, X. Li, Z. Bai, J. Yang, D. Xiong, D. Li, *J. Mater. Chem. A* 3 (2015) 11773.
2. J. Mosa, J.F. Velez, I. Lorite, N. Arconada, M. Aparicio, *J. Power Sources* 205 (2012) 491.
3. K. Mukai, Y. Kato, H. Nakano, *J. Phys. Chem. C* 118 (2014) 2992.
4. D.V. Safronov, S.A. Novikova, A.M. Skundin, A.B. Yaroslavtsev, *Inorg. Mater.* 48 (2012) 57.
5. B.T. Zhao, R. Ran, M.L. Liu, Z.P. Shao, *Meter. Sci. Eng. R* 98 (2015) 1.
6. L. Sun, J. Wang, K. Jiang, S. Fan, *J. Power Sources* 248 (2014) 265.
7. J. Cheng, R. Che, C. Liang, J. Liu, M. Wang, J. Xu, *Nano Res.* 7 (2014) 1043.
8. Y. Zhao, J. Sun, X. Chen, H. Zhu, W. Yang, *New J. Chem.* 38 (2014) 1173
9. A. Nugroho, K.Y. Chung, J. Kim, *J. Phys. Chem. C* 118 (2014) 183.
10. A.K. Haridas, C.S. Sharma, T.N. Rao, *Small* 11 (2015) 290.
11. A. Izumi, M. Sanada, K. Furuichi, K. Teraki, T. Matsuda, K. Hiramatsu, H. Munakata, K. Kanamura, *J. Power Sources* 256 (2014) 244.
12. Y. Wu, H. Wu, S. Luo, K. Wang, F. Zhao, Y. Wei, P. Liu, K. Jiang, J. Wang, S. Fan, *RSC Adv.* 4 (2014) 20010.
13. S. W. Han, S.J. Kim, E.S. Oh, *J. Electrochem. Soc.* 161 (2014) A587.
14. G.M. Zhou, F. Li, H.M. Cheng, *Energy Environ. Sci* 7 (2014) 1307.
15. B.T. Zhao, G.M. Yang, R. Ran, C. Kwak, D.W. Jung, H.J. Park, Z.P. Shao, *J. Mater. Chem. A* 2 (2014) 9126.
16. J.H. Choi, W.H. Ryu, K. Park, J.D. Jo, S.M. Jo, D.S. Lim, I.D. Kim, *Sci. Rep.* 4 (2014) 7334.
17. J. Liu, K. Song, P.A. van Aken, J. Maier, Y. Yu, *Nano Lett.* 14 (2014) 2597.
18. X. Wang, B. Liu, X. Hou, Q. Wang, W. Li, D. Chen, G. Shen, *Nano Res.* 7 (2014) 1073.
19. L. Gao, S. Li, D. Huang, Y. Shen, M. Wang, *J. Mater. Chem. A* 3 (2015) 10107.
20. S. Cao, X. Feng, Y. Song, X. Xue, H. Liu, M. Miao, J. Fang, L. Shi, *ACS Appl. Mater. Interfaces* 7 (2015) 10695.
21. Y. J. Gu, Z. Guo, H. Q. Liu, *Electrochim. Acta* 123 (2014) 576.
22. H. Hayashi, T. Nakamura, T. Ebina, *J. Ceram. Soc. Jpn.* 122 (2014) 78.
23. S.W. Han, J. Jeong, D.H. Yoon, *Appl. Phys. A: Mater. Sci. Process.* 114 (2014) 925.
24. D. Wang, X. Wu, Y. Zhang, J. Wang, P. Yan, C. Zhang, D. He, *Ceram. Int.* 40 (2014) 3799.
25. H. Xu, X. Hu, W. Luo, Y. Sun, Z. Yang, C. Hu, Y. Huang, *ChemElectroChem* 1 (2014) 611.
26. C.C. Yang, H.C. Hu, S.J. Lin, W.C. Chien, *J. Power Sources* 258 (2014) 424.
27. J.G. Kim, M.S. Park, S.M. Hwang, Y.U. Heo, T. Liao, Z. Sun, J.H. Park, K.J. Kim, G. Jeong, Y.J. Kim, J.H. Kim, S.X. Dou, *ChemSusChem* 7 (2014) 1451.
28. V.D. Nithya, S. Sharmila, K. Vediappan, C.W. Lee, L. Vasylechko, R.K. Selvan, *J. Appl. Electrochem.* 44 (2014) 647.
29. T.F. Yi, S.Y. Yang, X.Y. Li, J.H. Yao, Y.R. Zhu, R.S. Zhu, *J. Power Sources* 246 (2014) 505.
30. K. Song, D.H. Seo, M.R. Jo, Y.I. Kim, K. Kang, Y.M. Kang, *J. Phys. Chem. Lett.* 5 (2014) 1368.

31. C.W. Xiao, Y. Ding, J.T. Zhang, X.Q. Su, G.R. Li, X.P. Gao, P.W. Shen, *J. Power Sources* 248 (2014) 323.
32. Q. Zhang, H. Lu, H. Zhong, X. Yan, C. Ouyang, L. Zhang, *J. Mater. Chem.* A 3 (2015) 13706.
33. X. Li, S. Tang, M. Qu, P. Huang, W. Li, Z. Yu, *J. Alloys Compd.* 588 (2014) 17.
34. E.F. Rodriguez, F. Xia, D.H. Chen, A.F. Hollenkamp, R.A. Caruso, *J. Mater. Chem. A*, 4 (2016) 7772.
35. Q.Y. Zhang, M.G. Verde, J.K. Seo, X. Li, Y.S. Meng, *J. Power Sources*, 280 (2015) 355.
36. S.Y. Yang, J. Yuan, Y.R. Zhu, T.F. Yi, Y. Xie, *Ceramics International*, 41 (2015) 7073.
37. F. Zhao, P. Xue, H.H. Ge, L. Li, B.F. Wang, *J. Electrochem. Soc.*, 163 (2016) A690.
38. Y.L. Zhang, X.B. Hu, Y.L. Xu, C. Chen, *Solid State Ionics*, 276 (2015) 18.
39. T.F. Yi, J.Z. Wu, M. Li, Y.R. Zhu, Y. Xie, R.S. Zhu, RSC Adv., 5 (2015) 37367.
40. C. Wang, Z. Guo, W. Shen, Q. Xu, H. Liu, Y. Wang, *Adv. Funct. Mater.* 24 (2014) 5511.
41. Y.R. Zhu, T.F. Yi, H.T. Ma, Y.Q. Ma, L.J. Jiang, R.S. Zhu, *J. Chem. Sci* 126 (2014) 17.
42. M. Krajewski, M. Michalska, B. Hamankiewicz, D. Ziolkowska, K.P. Korona, J.B. Jasinski, M. Kaminska, L. Lipinska, A. Czerwinski, *J. Power Sources* 245 (2014) 764.
43. C. Cheng, H. Liu, X. Xue, H. Cao, L. Shi, *Electrochim. Acta* 120 (2014) 226.
44. N. Li, J. Liang, D. Wei, Y. Zhu, Y. Qian, *Electrochim. Acta* 123 (2014) 346.
45. L.P. Fan, X. Tan, T. Yu, Z.Q. Shi, *RSC Adv.*, 6 (2016) 26406.
46. J.E. Hong, R.G. Oh, K.S. Ryu, *J. Electrochem. Soc.*, 162 (2015) A1978.
47. C.H. Chen, R. Agrawal, C.L. Wang, *Nanomaterials*, 5 (2015) 1469.
48. Z.K. Fang, Y.R. Zhu, T.F. Yi, Y. Xie, *ACS Sustainable Chem. Eng.*, 4 (2016) 1994.
49. C. Lin, X. Fan, Y. Xin, F. Cheng, M.O. Lai, H. Zhou, L. Lu, *J. Mater. Chem.* A 2 (2014) 9982.
50. C. Chen, Y. Huang, C. An, H. Zhang, Y. Wang, L. Jiao, H. Yuan, *ChemSusChem* 8 (2015) 114.
51. Y. Wang, H. Rong, B. Li, L. Xing, X. Li, W. Li, *J. Power Sources* 246 (2014) 213.
52. C. Wang, H. Li, A. Fu, J. Liu, W. Ye, P. Guo, G. Pang, X.S. Zhao, *New J. Chem.* 38 (2014) 616.
53. X. Sun, M. Hegde, Y. Zhang, M. He, L. Gu, Y. Wang, J. Shu, P.V. Radovanovic, B. Cui, *Int. J. Electrochem. Sci.* 9 (2014) 1583.
54. M.M. Chen, X. Sun, Z.J. Qiao, Q.-Q. Ma, C.Y. Wang, *J. Alloys Compd.* 601 (2014) 38.
55. Y. Zhu, S. Murali, W. Cai, X. Li, J.W. Suk, J.R. Potts, R.S. Ruoff, *Adv. Mater.* 2 (2010) 3906.
56. N. Zhu, W. Liu, M. Xue, Z. Xie, D. Zhao, M. Zhang, J. Chen, T. Cao, *Electrochim. Acta* 55 (2010) 5813.
57. Y. Shi, L. Wen, F. Li, H.-M. Cheng, *J. Power Sources* 196 (2011) 8610.
58. H. Xiang, B. Tian, P. Lian, Z. Li, H. Wang, *J. Alloys Compd.* 509 (2011) 7205.
59. Q. Zhang, W. Peng, Z. Wang, X. Li, X. Xiong, H. Guo, Z. Wang, F. Wu, *Ionics* 19 (2013) 717.
60. A.K. Rai, J. Gim, S.-W. Kang, V. Mathew, A. Ly Tuan, J. Kang, J. Song, B.J. Paul, J. Kim, *Mater. Chem. Phys.* 136 (2012) 1044.
61. X. Guo, H.F. Xiang, T.P. Zhou, W.H. Li, X.W. Wang, J.X. Zhou, Y. Yu, *Electrochim. Acta* 109 (2013) 33.
62. Y. Oh, S. Nam, S. Wi, J. Kang, T. Hwang, S. Lee, H.H. Park, J. Cabana, C. Kim, B. Park, *J. Mater. Chem. A* 2 (2014) 2023.
63. D.A.C. Brownson, D.K. Kampouris, C.E. Banks, *J. Power Sources* 196 (2011) 4873.
64. Q. Zhang, W. Peng, Z. Wang, X. Li, X. Xiong, H. Guo, Z. Wang, F. Wu, *Solid State Ionics* 236 (2013) 30.
65. D.R. Dreyer, S. Park, C.W. Bielawski, R.S. Ruoff, *Chem. Soc. Rev.* 39 (2010) 228.
66. J. X. Zhang, H. Q. Cao, X. L. Tang, W. F. Fan, G. C. Peng, M. Z. Qu, *J. Power. Sources*, 241 (2013) 619.
67. J.X. Zhang, Z.W. Xie, W. Li, S.Q. Dong, M.Z. Qu, *Carbon*, 74 (2014) 153.
68. Z.W. Xie, X. Li, W. Li, M.Z. Chen, M.Z. Qu, *J. Power. Sources*, 273 (2015) 754.
69. W. Li, H. Wang, M.Z. Chen, J. J. Gao, X. Li, W.J. Ge, M.Z. Qu, A.J. Wei, L. H. Zhang, Z. F. Liu, *Electrochimi. Acta*, 188 (2016) 499.

70. Y.B. He, F. Ning, B.H. Li, Q.S. Song, W. Lv, H.D. Du, D.Y. Zhai, F.Y. Su, Q.H. Yang, F.Y. Kang, *J. Power. Sources*, 202 (2012) 253.
71. H.F. Xiang, B.B. Tian, P.C. Lian, Z. Li, H.H. Wang, *J. Alloys Compd.* 509 (2011) 7205.